Extracting 3D Mode Shapes from Cell Phone Videos

Shawn Richardson, Mark Richardson
Vibrant Technology, Inc., Centennial, CO

Click here for the IMAC Power Point presentation.

ABSTRACT

Most power plants, oil refineries, and manufacturing plants worldwide have implemented machinery health monitoring programs for assessing the health of their rotating machinery and associated equipment. Digital vibration signals are the primary data used to detect and diagnose mechanical faults in machinery and equipment. A cell phone is a low-cost, non-contacting measurement device that can be used to accurately record the vibration of a machine during its operation. Everyone has a cell phone handy for making vibration measurements.

In this paper, it is shown how 3-dimensional (**3D**) Operational Modal Analysis (**OMA**) mode shapes of a rotating machine are calculated from a cell phone video using two curve fitting steps. First, the 2-dimensional (**2D**) **OMA** mode shapes of the machine are obtained by curve fitting a set of **ODS-FRFs** which were calculated from **TWFs** extracted from a cell phone video.

In the second step, **3D FEA** mode shapes of the machine are curve-fit to the **2D OMA** mode shapes to create **3D OMA** mode shapes. Starting with a cell phone video, this two-step curve fitting process yields accurate **3D OMA** mode shapes that can be used to characterize and diagnose the health of rotating machinery. This is demonstrated in a companion paper [1].

KEY WORDS

Time Waveform (**TWF**), Digital Fourier Transform (**DFT**), Operational Modal Analysis (**OMA**) mode shape, Finite Element Analysis (**FEA**) mode shape, Operating Deflection Shape (**ODS**), Degree of Freedom (**DOF**), Auto Power Spectrum (**APS**), Cross Power Spectrum (**XPS**), **ODS-FRF** (**APS** and **Phase** of an **XPS**), Structural Dynamics Modification (**SDM**).

ROTATING MACHINE

In a previous paper [2], **ODS's** were extracted from cell phone videos ***for nine different unbalance cases*** of the rotating machine shown in Figure 1. This machine has a variable speed motor connected to the rotor with a rubber belt. The motor speed was adjusted so that the rotor speed was ***approximately* 1000 RPM** throughout all the cell phone video recordings. The video from one of those ***nine different unbalance cases*** was used for this paper.

Figure 1. Rotating Machine & Unbalance Screws Added to Its Rotors

INTRODUCTION

In previous papers [1] - [3] we illustrated the use of a new method for extracting vibration **TWFs** from frames of a cell phone video. In this paper we introduce a two-step curve fitting process for calculating **3D** mode shapes of a rotating machine from the **2D** mode shapes calculated from a cell phone video.

In the first curve fitting step, the **2D** mode shapes of the machine are obtained by using traditional digital signal processing methods together with **FRF-based** curve fitting. In the second curve fitting step, **3D** mode shapes of the machine are calculated by curve fitting its **2D** mode shapes with **3D FEA** mode shapes. To perform this second curve fitting step, a simple **FEA** model of the rotating machine was constructed in three steps using the Structural Dynamics Modification (**SDM**) method [4].

To calculate the **FEA** mode shapes, first an **FEA** model of one of the bearing blocks of the machine was created, and its **FEA** mode shapes were calculated. Then an **FEA** model of the baseplate was created, and its **FEA** mode shapes were calculated.

Next, ***very stiff* FEA springs** were attached between both bearing blocks and the baseplate, as shown in Figure 8. Then **SDM** was used to calculate the new mode shapes of the two bearing blocks firmly attached to the base plate. One of the new mode shapes is shown in Figure 8. Finally, **FEA** spring elements were attached between the corners of the baseplate and the fixed tabletop on which the rotating machine rested, and the new mode shapes of that model were calculated using **SDM** again.

Finally, a second curve fitting step was used to calculate the **3D OMA** mode shapes of the rotating machine from its **2D OMA** mode shapes. The **2D OMA** mode shapes were obtained by curve fitting the **ODS-FRFs** which were calculated from the cell phone video.

This two-step curve fitting process, curve fitting **ODS-FRFs** followed by curve fitting the **2D OMA** mode shapes with **3D FEA** mode shapes, can be used to calculate the **3D OMA** mode shapes of any rotating machine or test article when a cell video of it is recorded while it is vibrating.

TWFs & DFTs

A rectangular grid of points with rectangular surfaces attached between them is created when a video is processed in MEscope [8]. Frames of the video are attached to this surface during animated display of Video **ODS's**. Using a rectangular point grid, ***millions of pixels*** in each frame of a cell phone video are processed to extract **TWFs** for the horizontal & vertical deflections of ***thousands of points*** in the point grid. Grid points with ***little or no motion,*** (like background points), are hidden and their linked **TWFs** are removed from further analysis. A point grid with background points hidden is shown in Figure 2.

A **DFT** is calculated from each **TWF** that is extracted from the video. **Time-based ODS's** are displayed in animation from the **TWFs** using a sweeping Line cursor. **Frequency-based ODS's** are displayed in animation from the **DFTs** using sine dwell modulation of the **ODS** at the cursor position. The **magnitude & phase** of the **ODS** at selected grid points can also be displayed, as shown in Figure 2.

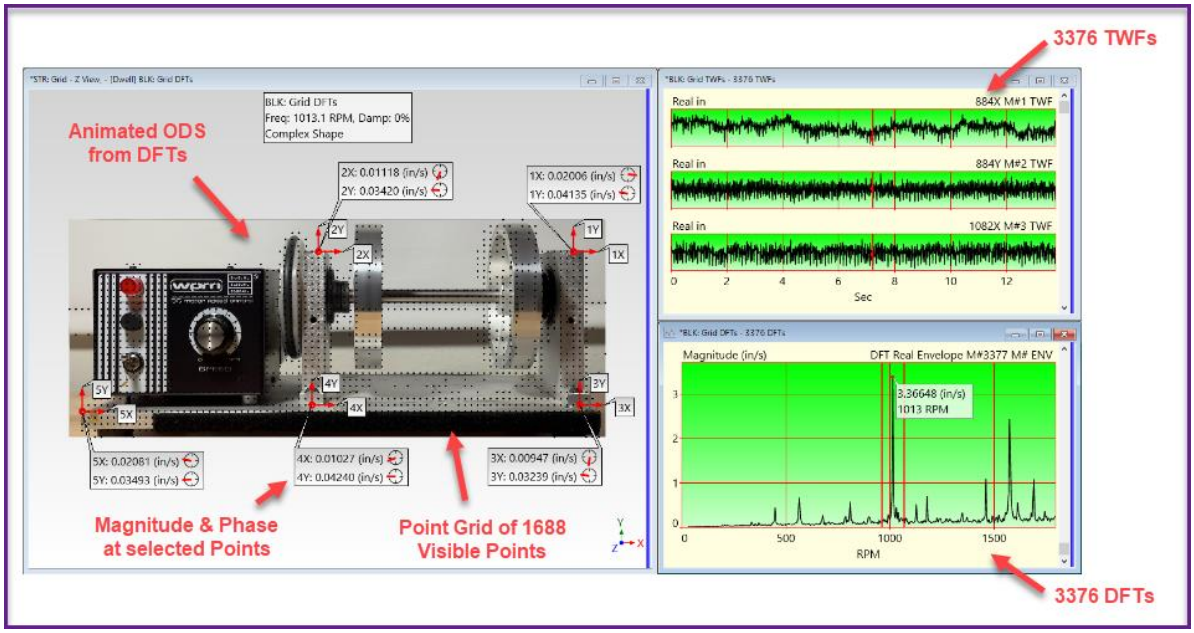

Figure 2. First-Order ODS Animated from DFTs

ODS-FRFs

A unique frequency domain function, called an **ODS-FRF,** can be calculated from each response **TWF** extracted from a video. A set of **ODS-FRFs** calculated from the **TWFs** is typically more accurate than **DFTs** because ***spectrum averaging*** can be used to reduce extraneous noise from the **ODS-FRFs**.

The ***magnitude*** of an **ODS-FRF** is the **APS** of the ***response*** **DOF** at a grid point. The ***phase*** of the **ODS-FRF** is the ***phase of the*** **XPS** between the ***response*** **DOF** and the **DOF** of any ***reference*** grid point.

ODS-FRFs carry the ***same displacement units*** as the response **TWFs** from which they are calculated. But because it is a frequency domain function, an **ODS-FRF** can be ***accurately differentiated to velocity units*** by multiplying it by the frequency variable.

Vibration in ***velocity units*** is commonly used by vibration analysts to quantify vibration levels in rotating equipment.

One of the laws of the **FFT** algorithm is that **Δf = 1/T**, where **Δf** is the ***frequency difference between samples*** of an **ODS-FRF**, and **T** is the ***time length*** of **TWF** data from which the **ODS-FRF** was calculated. For example, if an **ODS-FRF** is calculated from **TWF** data over a **15 second** period, the frequency resolution (**Δf**) of the **ODS-FRF** is **60/15 = 4 RPM**.

To increase the frequency resolution of an **ODS-FRF**, **TWF** data over a ***longer period*** **T** is required. Therefore, the video from which the **TWFs** are extracted must be recorded over a ***longer period*** **T**.

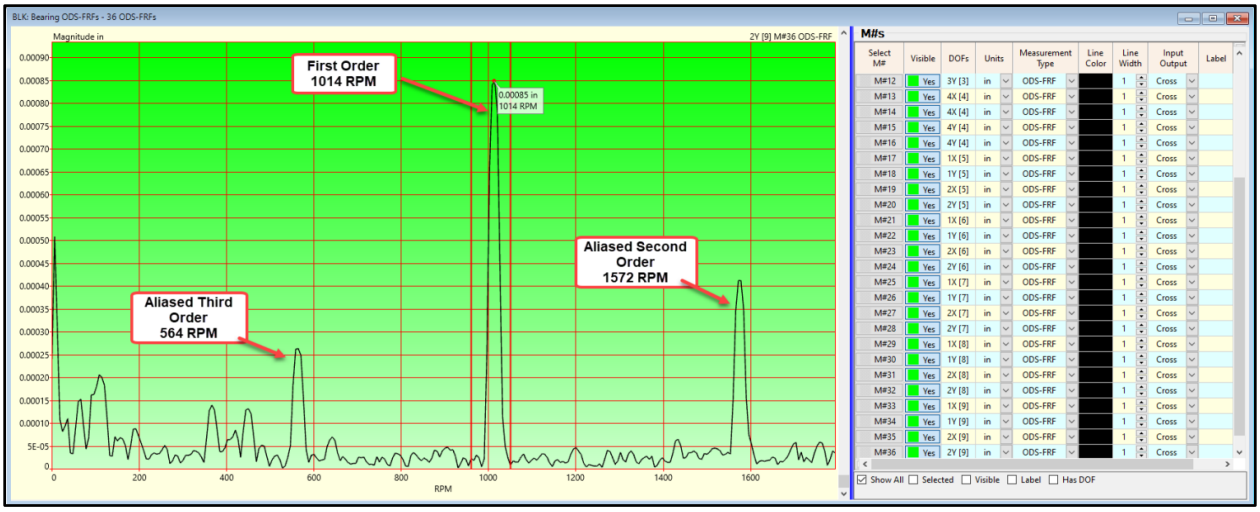

Figure 3. ODS-FRF Showing First Three Order Peaks.

ALIASED ORDER PEAKS

A limitation of any video recording is that ***anti-alias filtering cannot be used*** to remove high-frequency signals from the video.

Without anti-alias filtering, machine order peaks ***greater than one-half the sampling frequency***, (called **Fmax)**, are ***folded around*** **Fmax** and appear at lower frequencies in the **ODS-FRFs**, as shown in Figure 3.

All machine-order resonance peaks between **Fmax & 2x Fmax** are folded around (***wrapped around***) **Fmax** and appear at lower frequencies in the frequency band **(0 to Fmax)**. Aliasing of higher frequencies occurs in both **DFTs** and **ODS-FRFs**.

The **ODS-FRF** shown in Figure 3 was calculated from a **TWF** that was extracted from a video that was sampled at **60 fps**, or **3600 RPM**. Therefore, the **Fmax** of the **ODS-FRF** is **1800 RPM**. The first-order peak is at the machine running speed and is clearly visible at **1014 RPM**. The second order resonance peak should be at **2028 RPM** and third order resonance peak should be at **3042 RPM,** but they are both ***folded around*** **1800 RPM** and are clearly visible ***at lower frequencies*** in the **ODS-FRF**.

The aliased frequency of an order higher than **Fmax** can be calculated from **Fmax** and the expected order frequency.

- **Second order** aliased frequency ➔ 1800 - (2028 - 1800) ➔ **1572 RPM**
- **Third order** aliased frequency ➔ 1800 - (3042 - 1800) ➔ **558 RPM**

The **ODS-FRF** in Figure 3 was calculated from a **TWF** with ***a 10-second length***. Therefore **Δf = (1/10) Hz or 60/10 = 6 RPM** and the aliased frequency of the third order peak is ***within one*** **(Δf)** of its calculated value.

CURVE FITTING THE ODS-FRFS

ODS-FRFs can be curve-fit using an **FRF-based** curve fitter if they have been filtered with a special window. In MEscope [8] this filter is called a ***DeConvolution window***. This filter reshapes an **ODS-FRF** so that it more closely resembles an **FRF** and therefore can be curve fit using **FRF-based** curve fitting. An **FRF-based** curve fit of an **ODS-FRF** is shown in Figure 4. In the upper left-hand graph, the **red curve fitting function** is overlaid on a magnitude plot of the **ODS-FRF**.

The aliased frequencies of the second and third orders are correctly estimated by curve fitting the **ODS-FRFs**.

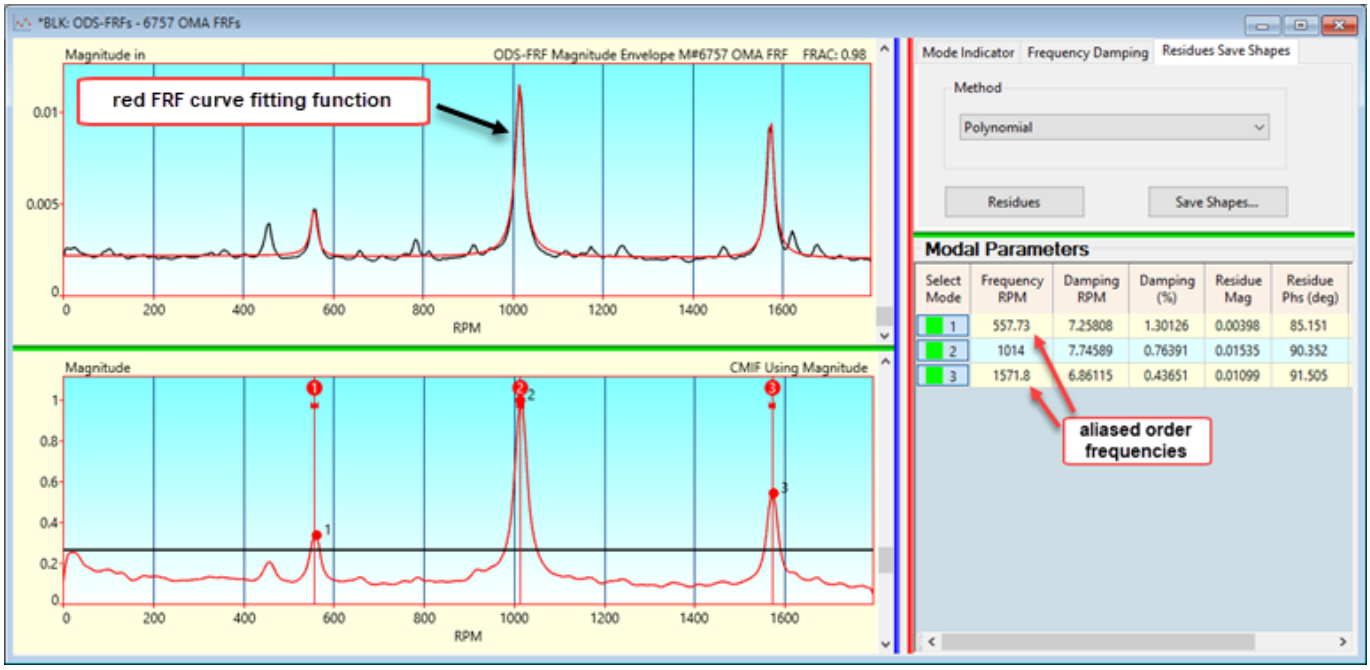

Figure 4. Curve Fit of ODS-FRFs.

DAMPING REMOVAL

DeConvolution windowed is necessary before using an **FRF-based** curve fitter on a set of **ODS-FRFs**. But DeConvolution windowing ***adds a known amount of damping*** to each **OMA** mode shape. Therefore, following **FRF-based** curve fitting, when the **OMA** mode shapes are stored into a Shape Table in MEscope [8], the damping added by DeConvolution windowing is removed from them. This is shown in Figure 5.

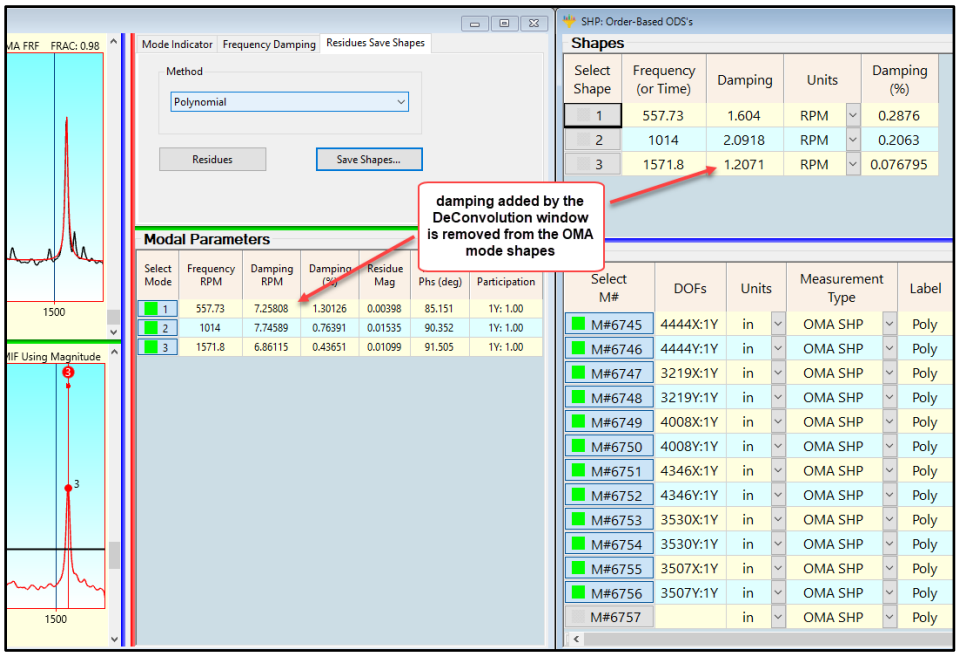

Figure 5. DeConvolution Window Damping is Removed when OMA Mode Shapes are Saved.

ANIMATING THE OMA MODE SHAPES ON THE POINT GRID

After the **2D OMA** modes shapes are saved in a Shape Table, they can be differentiated from ***displacement to velocity*** units. The three **OMA** mode shapes are shown in figure 6.

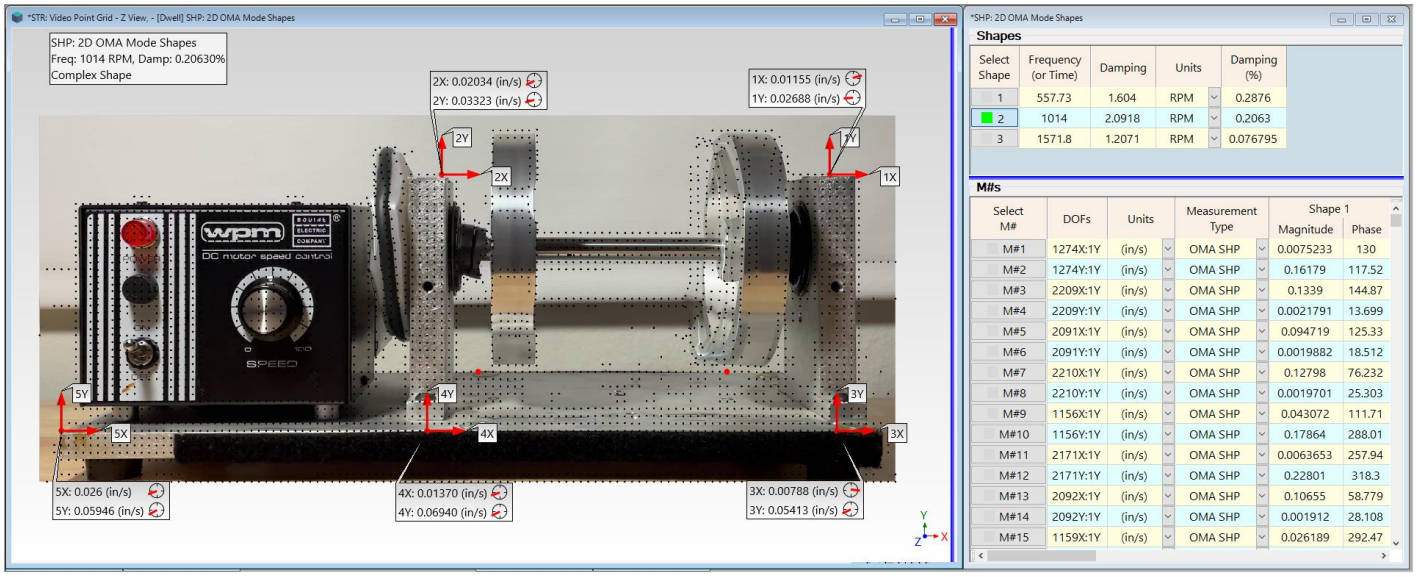

Figure 6. Animated Display of 1014 RPM OMA Mode Shape on the Point Grid

STRUCTURAL DYNAMICS MODIFICATION (SDM)

SDM [4] is a modeling algorithm also referred to as ***"eigenvalue modification"***. Starting with the mode shapes of an unmodified mechanical structure, **SDM** calculates the ***new mode shapes*** resulting from making ***physical modifications*** to the structure by adding **FEA** elements between points on a model of the structure. Modifications are modeled with industry-standard finite elements. The inputs and outputs of **SDM** are depicted in Figure 7.

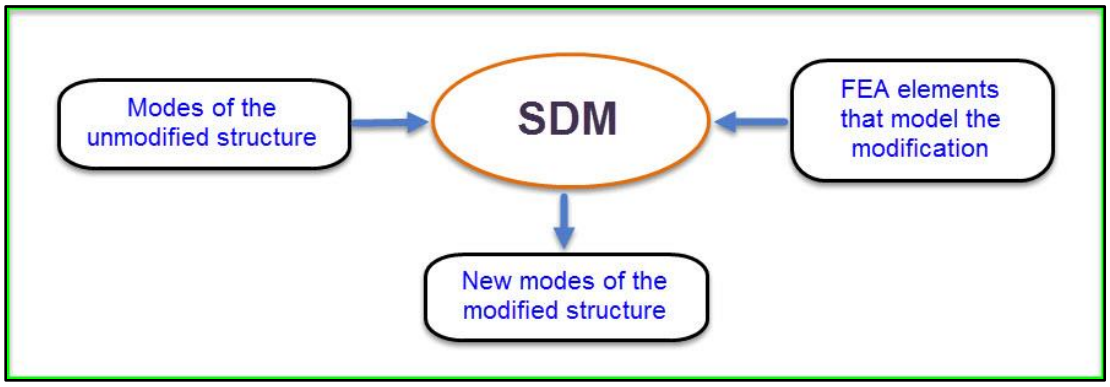

Figure 7. Structural Dynamics Modification (SDM)

FEA MODE SHAPES

The mode shapes of an **FEA** model of the baseplate & bearing blocks of the machine with rubber mounts resting on a fixed tabletop were calculated in three steps. First, an **FEA** model of a single bearing block was created, and its **FEA** mode shape**s** were calculated. Then, an **FEA** model of the baseplate was created, and its **FEA** mode shapes were calculated. Then **SDM** was used to model the attachment of both bearing blocks to the baseplate using ***very stiff*** **FEA spring elements**. This is depicted in Figure 8.

Next, to model the machine resting on a ***fixed*** tabletop, four **FEA spring elements** were added between each corner of the baseplate and a ***fixed ground point*** below the corner. Then **SDM** was used again to calculate the **FEA** mode shapes of the machine resting on the tabletop, as shown in Figure 9.

A stiffness of **10,000 lbs/inch** was used for each of the corner **FEA** spring elements. Using a different stiffness would change the frequencies of the **FEA** modes, but not their mode shapes. Only the **3D FEA** mode shapes are used to curve fit the **2D OMA** mode shapes, not their frequencies.

Admittedly, a much more accurate **FEA** model of the rotating machine could be created, but the **3D** mode shapes of this simplified model are sufficient for calculating **3D OMA** mode shapes by curve fitting the **2D OMA** mode shapes of the machine.

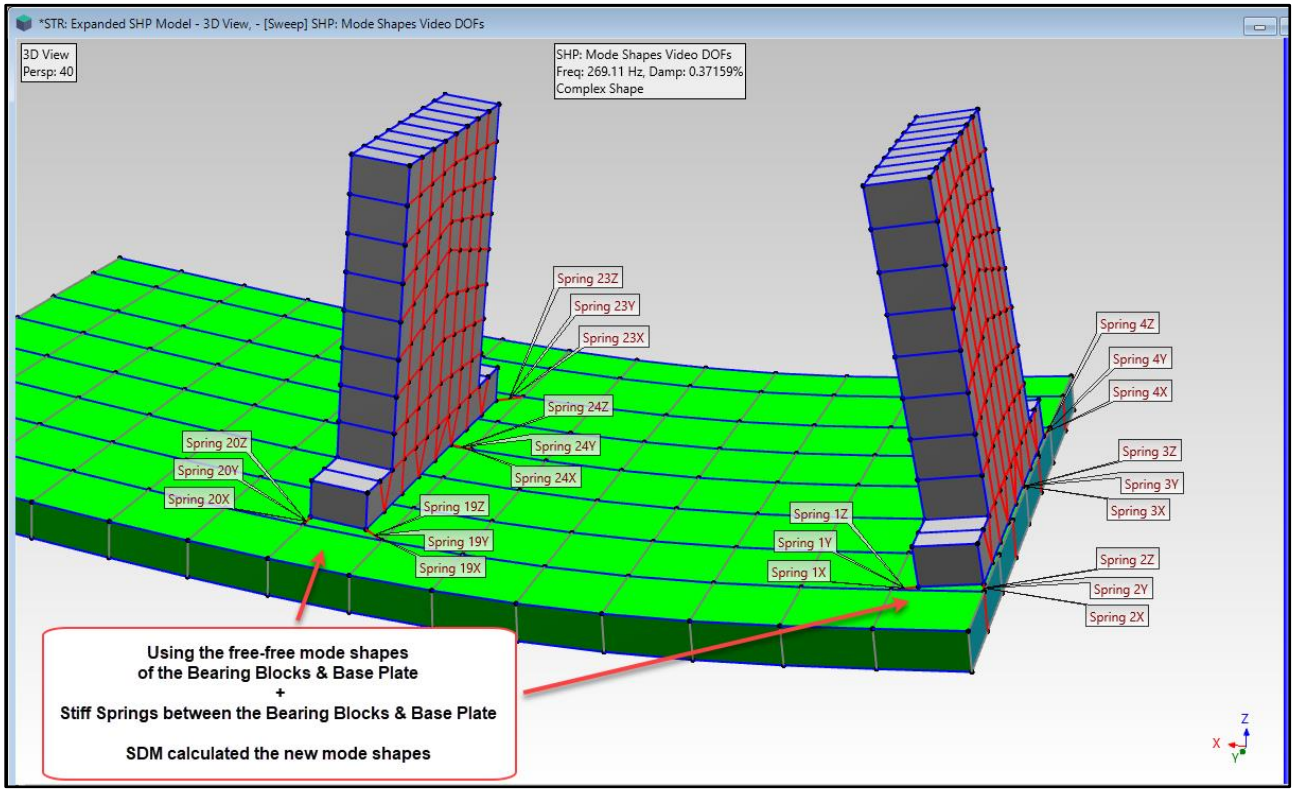

Figure 8. Bearing Blocks Attached to the Baseplate With Very Stiff FEA Springs

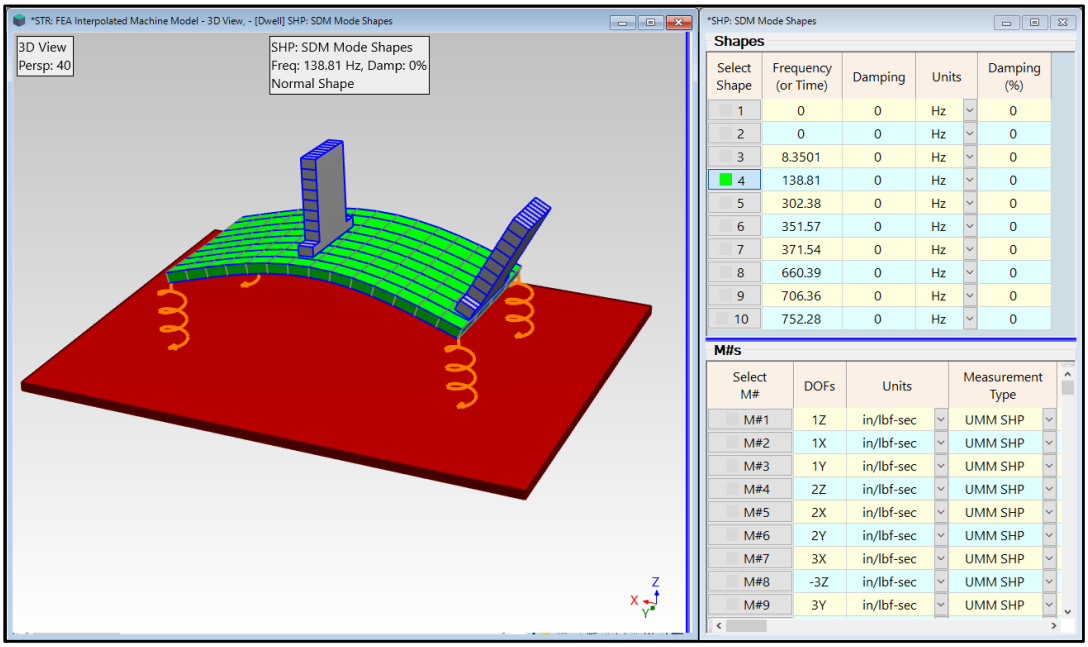

Figure 9. Baseplate & Bearing Blocks Attached to the Fixed Tabletop With FEA Springs.

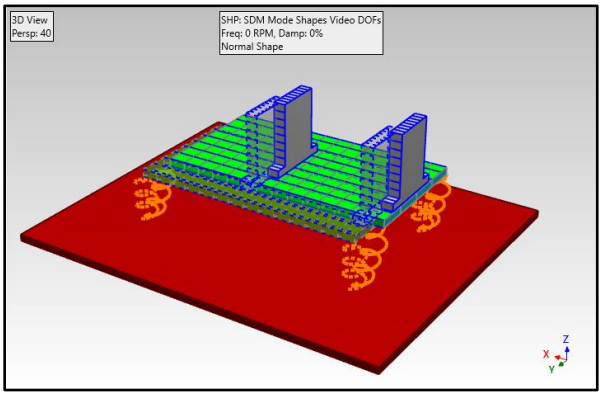

Mode 1-Rigid-Body Mode Shape

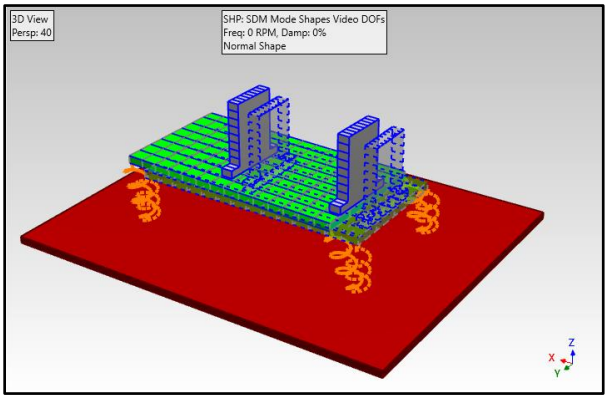

Mode 2-Rigid-Body Mode Shape

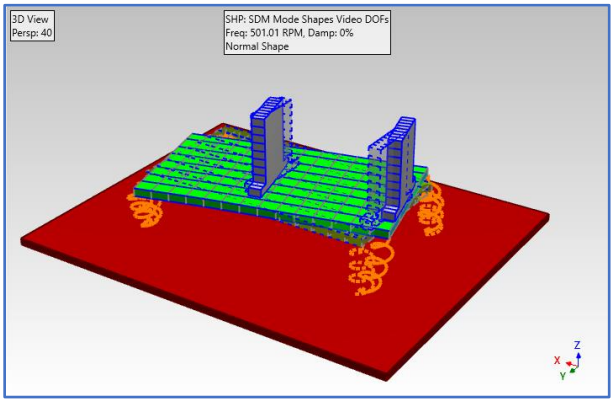

Mode 3 -Rigid-Body Mode Shape

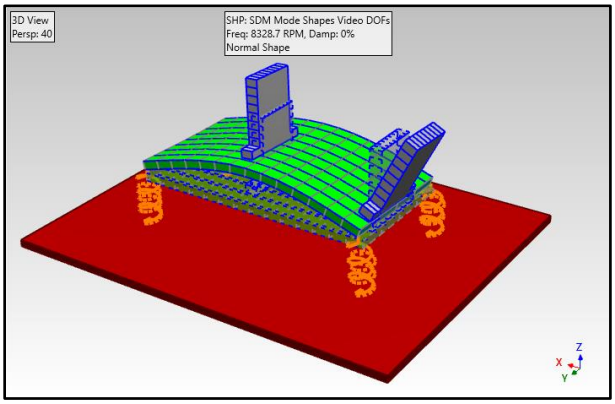

Mode 4-Flexible-Body Mode Shape

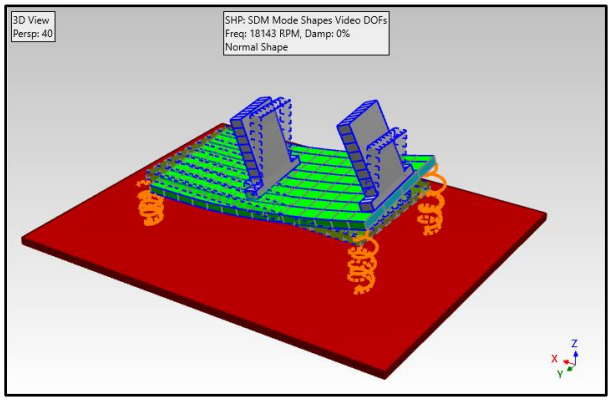

Mode 5-Flexible-Body Mode Shape

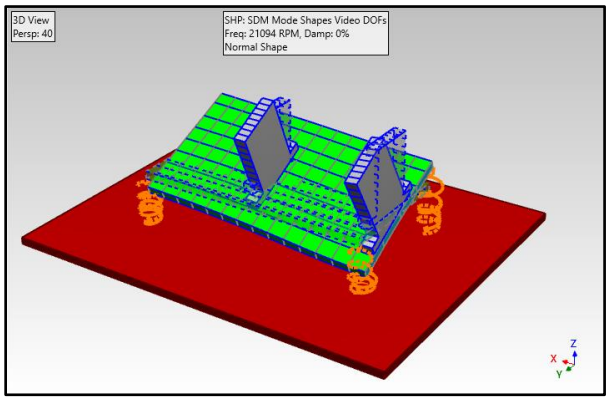

Mode 6-Flexible-Body Mode Shape

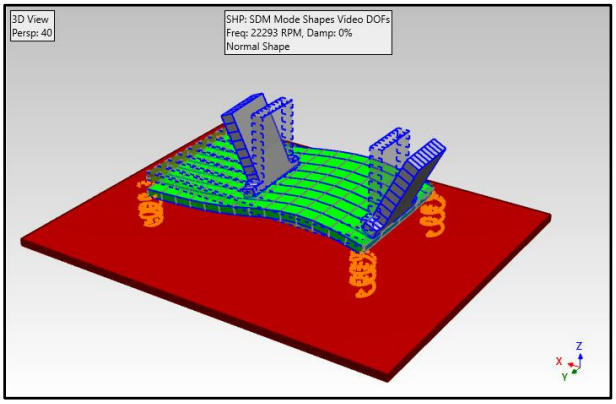

Mode 7-Flexible-Body Mode Shape

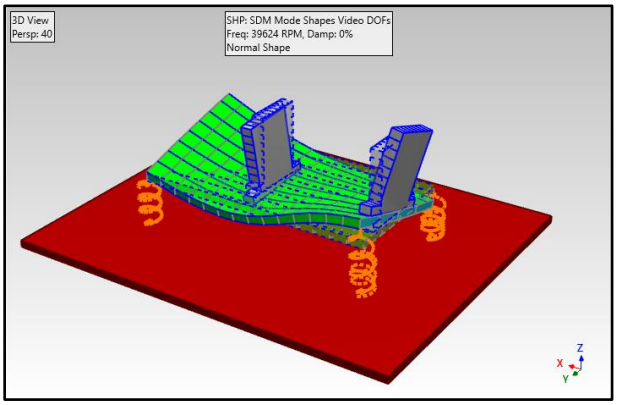

Mode 8-Flexible-Body Mode Shape

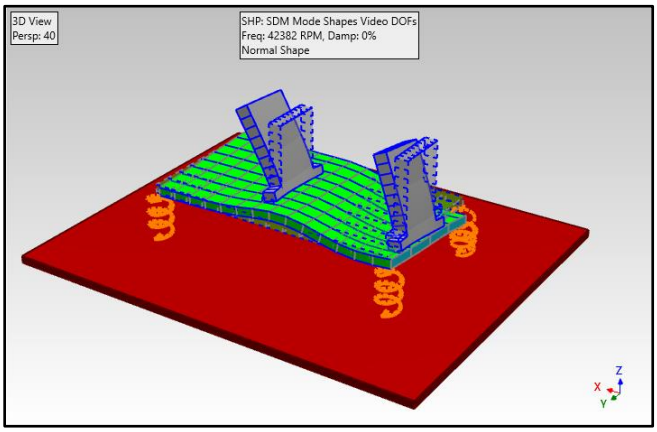

Mode 9-Flexible-Body Mode Shape

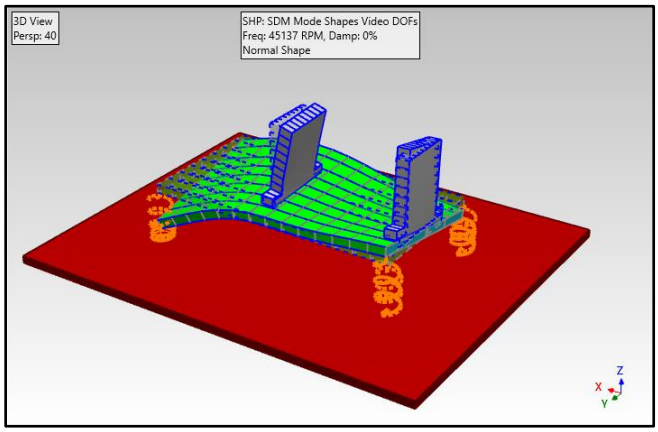

Mode 10-Flexible-Body Mode Shape

Figure 10. FEA Mode Shapes of the Baseplate & Bearing Blocks on a Fixed Base

The ***ten lowest-frequency*** **FEA** mode shapes of the machine resting on a fixed tabletop with rubber mounts are shown in Figure 10.

Since damping was not modeled in the **FEA** models, all the mode shapes shown in Figure 10 have ***zero damping*** in them.

The ***first two*** mode shapes also have ***zero frequency***, and the ***third mode*** has a frequency ***nearly equal to zero.*** Since there is no bending of them in the baseplate or bearing blocks, these first three mode shapes in Figure 10 are called ***rigid-body*** mode shapes.

The first three mode shapes exhibit ***rigid-body*** deflection of the machine on its rubber mounts. The first two mode shapes are ***translational*** deflections in two directions and the third mode shape is ***rotational*** motion on the rubber mounts. All the other higher-frequency modes exhibit bending of the baseplate & bearing blocks; hence they are called ***flexible-body*** mode shapes.

CURVE FITTING FEA MODE SHAPES TO 2D OMA MODE SHAPES

In this second curve fitting step **3D OMA** mode shapes are calculated by curve fitting the **3D FEA** mode shapes of the machine to its **2D OMA** mode shapes. The **3D FEA** mode shapes of the baseplate & bearing blocks mounted with springs to a fixed base are curve fit to the **2D OMA** mode shapes obtained from curve fitting the **ODS-FRFs**.

To curve fit the **3D** mode shapes to the **2D** mode shapes, five points on the video point grid were given the ***same point numbers*** as the ***five closest points*** on the **3D FEA** model, when viewed from the same direction as the video recording. The ***common numbered points*** are shown on the **FEA** model and on the point grid in Figure 11.

The **FEA** mode shapes were curve-fit to the experimental **OMA** mode shapes using ***10 common*** shape **DOFs**, horizontal & vertical deflection at each of the five common points. This ***least-squared-error*** curve fitting yields a complex-valued ***participation*** of each **3D FEA** mode shape in each **2D OMA** mode shape. Then the **3D OMA** mode shapes are calculated using the ***participation*** of each **FEA** mode shape in each **OMA** mode shape.

- The **2D OMA** mode shapes have **6756 DOFs** in them, defining the **X & Y** motion at **3378 visible points** in the point grid
- The **3D FEA** mode shapes have **1938 DOFs** in them, defining the **X, Y & Z** motion at **646 points** in the **FEA** model

These are typical numbers of points for a video point grid and a simple **FEA** model of the baseplate & bearing blocks connected to a fixed base with rubber mounts.

- ***Least-sqaured-error*** curve fitting was performed using the ***10 common*** **DOFs** between the **2D OMA** shapes and the **3D FEA** mode shapes
- **3D OMA** mode shapes were calculated using the ***participation*** of each **FEA** mode shape in each **OMA** mode shape

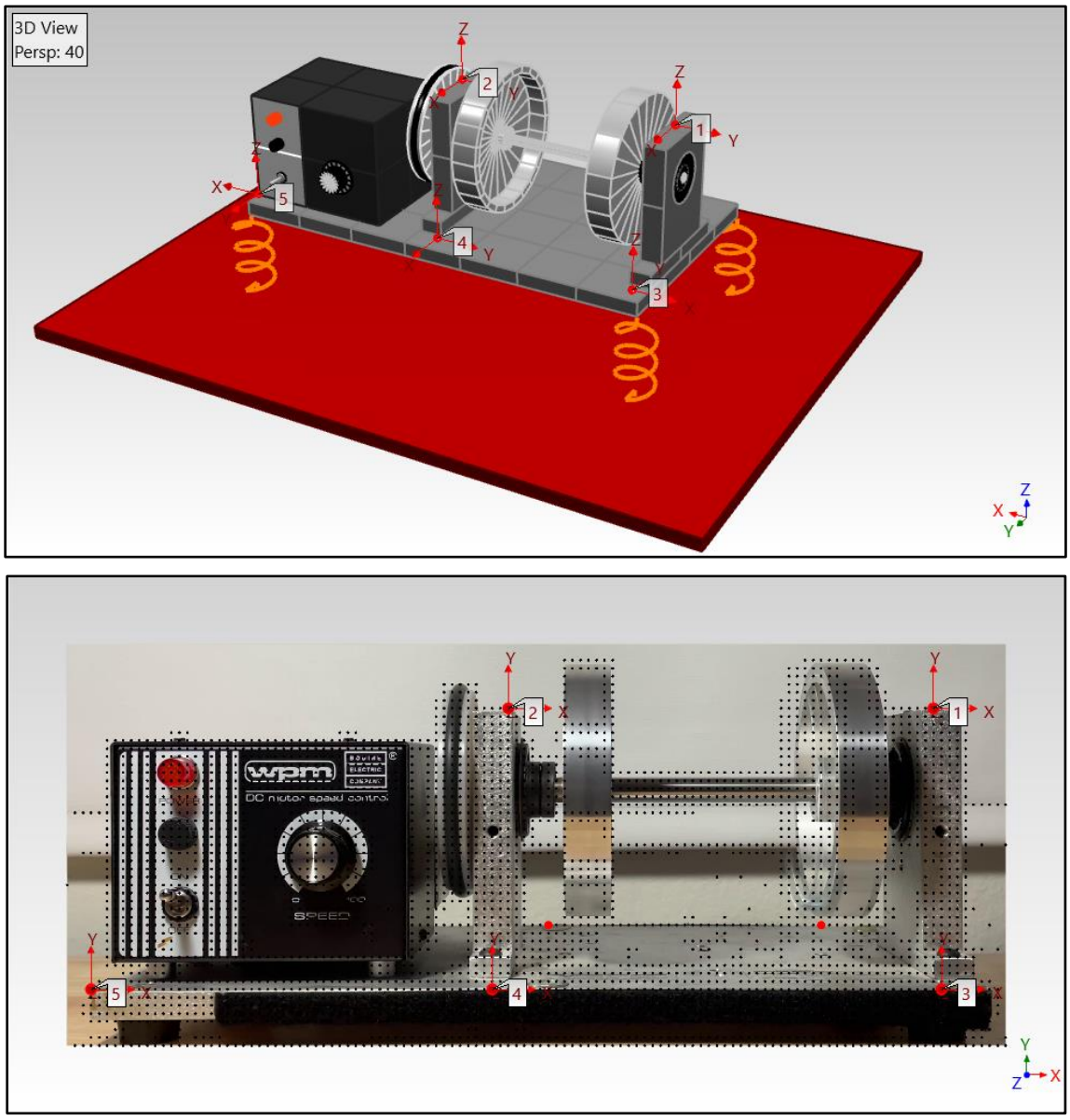

Figure 11. FEA Model and Video Point Grid Showing Five Common Points.

Points must be chosen on the **FEA** model which are ***"close"*** to being in the ***same plane*** as the points chosen in the video point grid. **2D** mode shape components from the **two red points** on the far side of the baseplate in the point grid cannot be used in this curve fitting step because ***their deflections would be less than the deflections*** of the **3D FEA** mode shapes at those corresponding points.

ANIMATED DISPLAY OF THE 3D OMA MODE SHAPES

Animation of the **3D OMA** mode shape of the first order at **1014 RPM** is shown in Figure 12. (Animated display shows the deflection of the mode shape more clearly.)

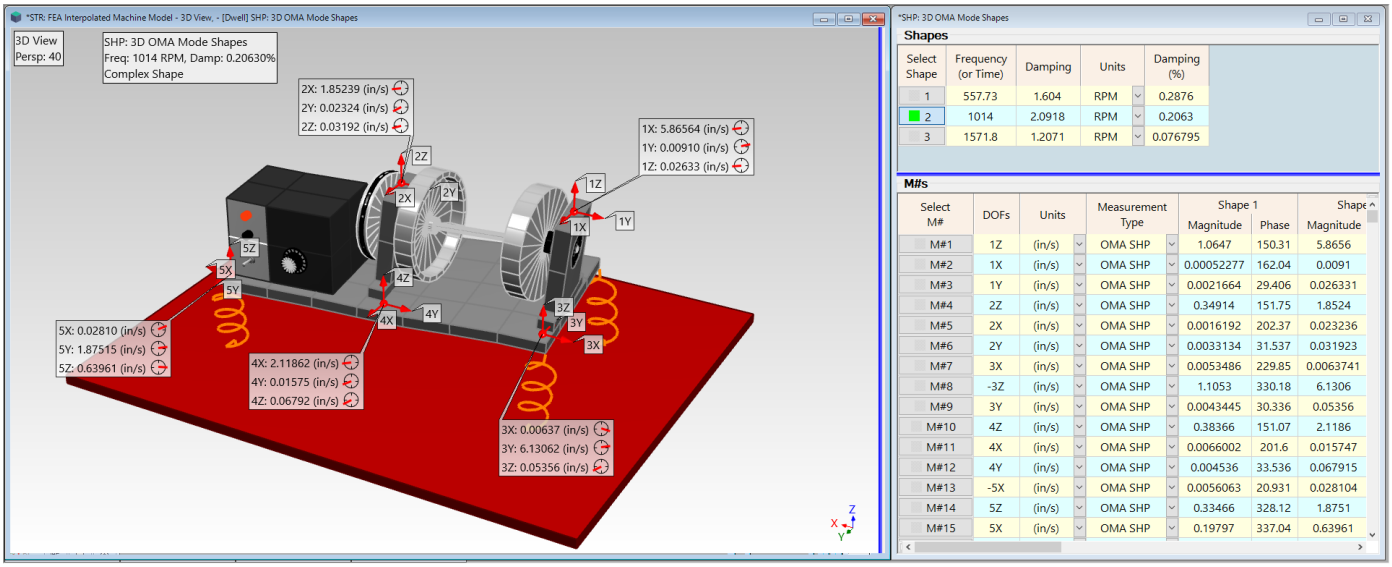

Figure 12. Animated Deflection of the First-Order OMA Mode Shape

MODAL PARTICIPATION

The participation of the **10 FEA** mode shapes in each **3D OMA** mode shape is shown in Figure 13. All the **3D OMA** mode shapes are ***very similar in shape*** because the **FEA** mode shapes ***participate nearly the same*** in each **3D OMA** mode shape, as shown in Figure 13. Only the ***magnitudes*** of the participation bars are different.

It can be concluded from Figure 13 that the mode shapes of the ***same three natural resonances dominate*** the first three orders of the machine's deflection at **1000 RPM**.

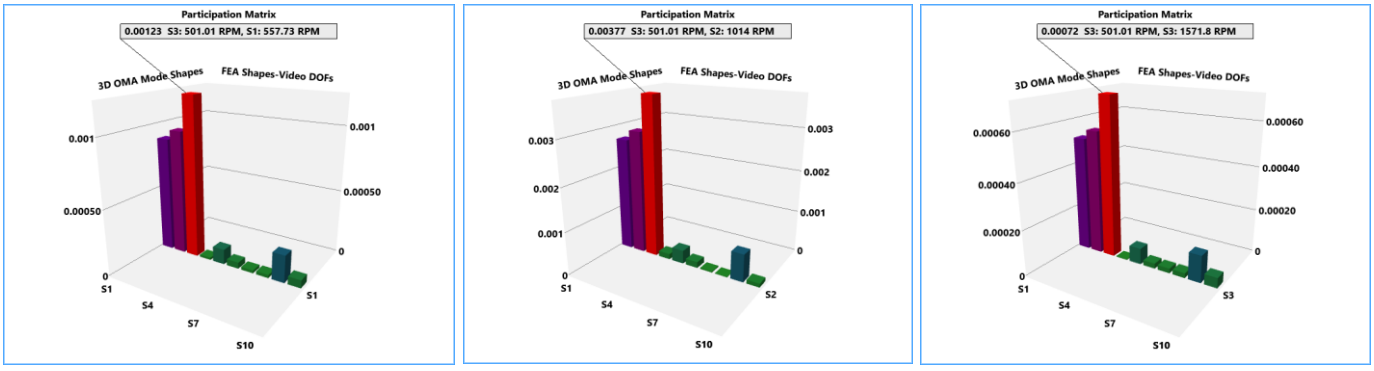

Figure 13. Participation of FEA Mode Shapes in Each Order-Based OMA Mode Shape

But re-examining the mode shapes in Figure 10, the first three **FEA** mode shapes define the ***rigid-body motion of the machine bouncing on its rubber mounts*** due to the unbalance forces from the rotors. All the remaining seven ***flexible-body*** mode shapes participate in the resonant vibration of the first three orders, with the ***sixth mode shape*** having the largest participation among the seven. From Figure 10 the deflection of the sixth resonance shows the entire machine ***rocking side-to-side*** on its rubber mounts. These results agree with our intuition.

CONCLUSIONS

In this paper, we introduced a new method for curve fitting the **2D** mode shapes of a rotating machine to obtain its **3D** mode shapes. First, **ODF-FRFs** were calculated from the **TWFs** that were extracted from a **16-second-long** cell phone video of the rotating machine. Then, **2D OMA** mode shapes of a rotating machine were obtained by applying **FRF-based** curve fitting to the **ODS-FRFs**.

The **ODS-FRFs** contained the peaks of the ***first three orders*** of the rotating machine, two of them aliased about the **1800 RPM Fmax** of the **ODS-FRFs**. The **2D OMA** mode shapes obtained by curve fitting the **ODS-FRFs** were the mode shapes of the first three machine orders.

Then **3D FEA** mode shapes of the bearing blocks & baseplate of the machine resting on springs attached to a fixed tabletop were calculated in a series of steps. First an **FEA** model of a bearing block was constructed, and its mode shapes were calculated. Likewise, an **FEA** model of the baseplate was constructed, and its mode shapes were calculated. Then both bearing blocks were attached to the baseplate using very stiff springs. Finally, **SDM** was used to calculate the mode shapes of the baseplate & bearing blocks resting with rubber mounts on a fixed tabletop.

Finally, **3D OMA** mode shapes of the machine were calculated in a second curve fitting step by curve fitting **10 FEA** mode shapes of the machine to the **2D OMA** mode shapes of the machine. The participation of each **FEA** mode shape in each **3D OMA** mode shape gave results that satisfied our intuition.

These results verify **one of the laws of modal analysis**, namely that,

- All vibration can be represented as a ***summation of mode shapes***

REFERENCES

[1] - S. Richardson, M. Richardson “Using Mode Shapes Derived from Cell Phone Videos to Monitor the Health of Rotating Machinery” IMAC XLII, January 29 - February 1, 2024, Orlando, FL.

[2] - B. Schwarz, S. Richardson, P. McHargue, M. Richardson “Using Modal Analysis and ODS Correlation to Identify Mechanical Faults in Rotating Machinery” IMAC XLII, January 29 - February 1, 2024, Orlando, TX.

[3] - D. Ambre, B. Schwarz, S. Richardson, M. Richardson, “Using Cell phone Videos to Diagnose Machinery Faults” IMAC XLI, , Austin, TX, February 13-16, 2023.

[4] - D. Formenti, M, Richardson, “Modal Modeling and Structural Dynamics Modification” Vibrant Technology, Inc., February 3, 2020.

[5] - B. Schwarz, S. Richardson, J. Tyler, R. Spears, M. Richardson, “Post-Processing ODS Data from a Vibration Video” IMAC XXXVIII Houston, TX, February 10-13, 2020.

[6] - B. Schwarz, M.H. Richardson, “Measurements Required for Displaying Operating Deflection Shapes” Proceedings of IMAC XXII, January 26, 2004

[7] - “B. Schwarz, P. McHargue, M. Richardson “Using SDM to Train Neural Networks for Solving Modal Sensitivity Problems” 14th IMAC Conference, Dearborn, MI, February 1996

[8] - MEscope™ is a trademark of Vibrant Technology, Inc. www.vibetech.com